Linearization of MIMO Multi-Band Transmitter in The Presence of Nonlinear Crosstalk

Amir Vaezi, Abdolali Abdipour, Abbas Mohammadi, , and Fadhel Ghannouchi.

A. Vaezi, is with the Micro/mm-wave and Wireless Communication Research Lab, Radio Communications Center of Excellence, Electrical Engineering Department, Amirkabir University of Technology, Tehran, Iran and also, with the Intelligent RF Radio Laboratory (iRadio Lab), Department of Electrical and Computer Engineering, University of Calgary, Calgary, AB, Canada

A. Abdipour and A. Mohammadi are with the Micro/mm-wave and Wireless Communication Research Lab, Radio Communications Center of Excellence, Electrical Engineering Department, Amirkabir University of Technology, Tehran, Iran.

F. Ghannouchi is with the Intelligent RF Radio Laboratory (iRadio Lab), Department of Electrical and Computer Engineering, University of Calgary, Calgary, AB, Canada T2N 1N4

Abstract—This paper proposes a digital pre-distortion (DPD) linearization technique for an N×N MIMO multi-band transmitter in the presence of nonlinear crosstalk. Nonlinear crosstalk refers to the signal leakage and coupling effect between the MIMO paths at the input of power amplifiers. In the proposed technique, the RF signal of each frequency band in each path is characterized and linearized separately. The performance of the proposed DPD is validated using a 2×2 MIMO setup including two power amplifiers driven by dual-band long-term evaluation (LTE) signals. Two scenarios are then considered in the presence of the crosstalk level of -20dB: a MIMO dual-band transmitter and a MIMO tri-band transmitter. The simulation and experimental results demonstrate a low normalized mean square error (NMSE) between the model and the measurement results. By applying the DPD a significant improvement in adjacent channel power ratio (ACPR) to less than -50 dBc is achieved.

Key words: multiple input multiple output (MIMO), digital pre-distortion (DPD), nonlinear crosstalk, multi-band, power amplifier.

1. INTRODUCTION

Currently multi-band wireless systems are highly demanding due to their flexibility and reconfigurability to support the different frequency bands simultaneously. Moreover, in multi-band systems, the interference and distortion effects between frequency bands degrade the overall system performance [1,2]. Those effects turn into a challenging issue in nonlinear devices and components such as power amplifiers (PA) and transmitters. Therefore, it is essential to consider the nonlinear inter-modulation distortion between frequency bands in order to provide an accurate model for multi-band PAs [1,3, 4]. On the other hand, deploying multi-band PAs in multiple-input multiple-output (MIMO) topology, which is known to suffer from the presence of crosstalk between the multiple paths, becomes more challenging [5].

Behavioral modeling and also digital pre-distortion (DPD) as an efficient method to compensate for the nonlinearity of the transmitter have been widely investigated. Several schemes of two-dimensional DPD are proposed for a concurrent dual-band transmitter in [6, 7, 8, 9]. Also, mitigation and compensation of nonlinear distortion in tri-band transmitters have been studied in [10, 11].

Furthermore, the modeling and linearization of MIMO transmitters with different complexities have been recently explored in [5], [12, 13, 14].

Authors in [5] classified the crosstalk and coupling effect in a MIMO system as either linear or nonlinear crosstalk depending on where crosstalk occurs. Nonlinear crosstalk refers to the coupling which takes place before the PA as the main source of nonlinearity in the system. Therefore, the RF signal passes through a nonlinear device. The main source of this type of crosstalk may be the coupling between MIMO paths where they are implemented on a same chipset or the RF leakage signal through the common local oscillators [15]. On the other hand, the coupling between antennas at the transmitter and receiver which occurs after PAs, introduces linear crosstalk. Based on [5], unlike linear type, nonlinear crosstalk cannot be compensated by the conventional matrix inversion at the receiver, and therefore, essentially, should be considered in nonlinear modeling.

In [5], a crossover DPD is introduced to compensate for nonlinear crosstalk and nonlinearity in MIMO systems. Moreover, the performance of several behavioral models for linearization of a MIMO transmitter in the presence of linear and nonlinear crosstalk is studied and compared in [14]. However, to the best knowledge of the authors, behavioral modeling and compensation for the impairments of the MIMO multi-band transmitter has not been reported yet. In the case of N×N MIMO B-band transmitter, the coupling effects of the MIMO paths must be taken into account in the nonlinear behavioral model as well as the interference effect between different frequency bands. Therefore, considering intermodulation terms between all the input signals leads to the employment of an N×B-dimensional memory polynomial. It is apparent that the model complexity can be extremely high.

In this paper, a less complex memory polynomial model and a DPD for linearization of the N×N MIMO multi-band system in the presence of nonlinear crosstalk are proposed. Since the envelope signals of each RF carrier are considered to develop the model, the signal processing is independent of the frequency separation of different bands. The performance of the model is experimentally evaluated for two different scenarios: a 2×2 MIMO dual-band transmitter and a 2×2 MIMO tri-band transmitter. The measured and simulated results show the ability of the DPD to model and compensate for the nonlinear and crosstalk impairments.

2. Modeling of MIMO Multi-band System

A. Modeling of MIMO dual-band transmitter

Nonlinear crosstalk which occurs at the input of PAs, is considered here. By considering a 2×2 MIMO dual-band system, the input signal of *i-th* branch can be expressed as:

$$\tilde{x}^{(i)} = u_{[n]}^{(i)} e^{-j\omega_n T} + v_{[n]}^{(i)} e^{+j\omega_n T} \quad i = 1,2 \qquad (1)$$

where $u_{[n]}^{(i)}$ and $v_{[n]}^{(i)}$ are the complex envelope of the input signals around the lower and upper frequency bands, respectively. The frequency spacing between bands is $2 \times \omega_n$. Consequently, the output signal of

the transmitter at the lower band of the first MIMO branch in the presence of nonlinear crosstalk can be modeled as follows:

$$y_{u\,[n]}^{(1)} = f^{(1)}\left(u_{[n]}^{(1)}, v_{[n]}^{(1)}, \alpha_i u_{[n]}^{(2)}, \beta_i\, v_{[n]}^{(2)}\right) \qquad (2)$$

where α_j and β_j are the impulse response of the coupling between MIMO paths. Since $f^{(1)}$ is a function of four different signals, a four-dimensional behavioral model is required to model these nonlinear functions. A model containing all cross-term combinations between all input signals can significantly increase the number of coefficients and model complexity. On the other hand, the typical value for crosstalk in transmitters is below -20 dB, and the leakage signals are very weak compared with the main input signal [5]. Therefore, in order to decrease the complexity, (2) can approximately be written as [12]:

$$y_{u\,[n]}^{(1)} = f_1^{(1)}\left(u_{[n]}^{(1)}, v_{[n]}^{(1)}\right) + f_2^{(1)}\left(u_{[n]}^{(2)},\ v_{[n]}^{(2)}\right) \qquad (3)$$

The output is expressed as a summation of two nonlinear functions, ($f_1^{(1)}$ and $f_2^{(1)}$),with each dependent on only the signals existing in each branch. Consequently, nonlinear functions in (3) can be replaced by the two-dimensional memory polynomial models. The two-dimensional memory polynomial is expressed as:

$$f_j\ \left(u_{[n]}, v_{[n]}\right) = \sum_{q=1}^{Q}\ \sum_{p=0}^{P}\ \sum_{k=0}^{p} C_{p,k,q}\ u_{[n-q]}\ \left|u_{[n-q]}\right|^{p-k}\left|v_{[n-q]}\right|^{k} \qquad (4)$$

where $C_{p,k,q}$ is the base-band polynomial complex coefficient, and *P* and *Q* are the maximum nonlinearity order and memory depth, respectively. Therefore, the relation between the input and output is proposed as:

$$y_{u\,[n]}^{(1)} = \sum_{q=1}^{Q}\ \sum_{p=0}^{P}\ \sum_{k=0}^{p} C_{u\,p,k,q}^{11}\, u_{[n-q]}^{(1)}\ \left|u_{[n-q]}^{(1)}\right|^{p-k}\left|v_{[n-q]}^{(1)}\right|^{k}$$

$$+\sum_{q=1}^{Q}\ \sum_{p=0}^{P}\ \sum_{k=0}^{p} C_{u\,p,k,q}^{12}\, u_{[n-q]}^{(2)}\ \left|u_{[n-q]}^{(2)}\right|^{p-k}\left|v_{[n-q]}^{(2)}\right|^{k} \qquad (5)$$

where $C_{u\,p,k,q}^{11}$ and $C_{u\,p,k,q}^{12}$ are the base-band polynomial complex coefficient related to the lower band signal. From (5), it is apparent that this model is composed of two 2D-memory polynomial terms regarding the intermodulation between the signals at each MIMO path. Following this process, the output signals of the transmitter at the upper band of the first MIMO branch, $y_{v\,[n]}^{(1)}$, as well as the signals for the second branch, $y_{u\,[n]}^{(1)}$ and $y_{v\,[n]}^{(2)}$ are extracted.

B. Modeling of MIMO tri-band transmitter

In a MIMO tri-band system, the input signal in each path contains three different signals in the lower, middle, and upper frequency bands determined by $u_{[n]}^{(i)}$, $v_{[n]}^{(i)}$, and $w_{[n]}^{(i)}$, respectively. Following the same procedure in the previous subsection, the output signal of the transmitter in the lower-band of the first path is given as:

$$y_{u\,[n]}^{(1)} = f_1^{(1)}\left(u_{[n]}^{(1)}, v_{[n]}^{(1)}, w_{[n]}^{(1)}\right) + f_2^{(1)}\left(u_{[n]}^{(2)}, v_{[n]}^{(2)}, w_{[n]}^{(2)}\right) \qquad (6)$$

Thus, in (6), a six-variable function is decomposed into two independent functions where each term can be modeled using a three-dimensional memory polynomial [10] as:

$$f_j\left(u_{[n]}, v_{[n]}\right) = \sum_{q=1}^{Q}\sum_{p=0}^{P}\sum_{s=0}^{p}\sum_{k=0}^{s} C_{p,s,k,q}\, u_{[n-q]}\left|u_{[n-q]}\right|^{p-s}\left|v_{[n-q]}\right|^{s-k}\left|w_{[n-q]}\right|^{k} \qquad (7)$$

Therefore, a 2×2 MIMO tri-band transmitter with nonlinear crosstalk is modeled as:

$$y_{u\,[n]}^{(1)} = \sum_{q=1}^{Q}\sum_{p=0}^{P}\sum_{s=0}^{p}\sum_{k=0}^{s} C_{u\,p,s,k,q}^{11}\, u_{[n-q]}^{(1)}\left|u_{[n-q]}^{(1)}\right|^{p-s}\left|v_{[n-q]}^{(1)}\right|^{s-k}\left|w_{[n-q]}^{(1)}\right|^{k} + \sum_{q=1}^{Q}\sum_{p=0}^{P}\sum_{s=0}^{p}\sum_{k=0}^{s} C_{j\,p,s,k,q}^{i2}\, u_{[n-q]}^{(2)}\left|u_{[n-q]}^{(2)}\right|^{p-s}\left|v_{[n-q]}^{(2)}\right|^{s-k}\left|w_{[n-q]}^{(2)}\right|^{k} \qquad (8)$$

As shown in (8), the tri-band model is an extended version of the dual-band model in (5).

C. *Generalized model for N×N MIMO multi-band transmitter*

In this subsection, based on the models presented in (5) and (8), a memory polynomial model for an N×N MIMO multi-band transmitter in the presence of nonlinear crosstalk is proposed. In this case, (3) can be extended to:

$$y_{j\,[n]}^{(i)} = \sum_{t=1}^{N} f_{t,j}\left(x_{1\,[n]}^{(t)}, \dots, x_{j\,[n]}^{(t)}, \dots, x_{B\,[n]}^{(t)}\right) \qquad (10)$$

where $x_{j\,[n]}^{(i)}$ and $y_{j\,[n]}^{(i)}$ represent the complex envelope input and output signals of the transmitter at *j-th* frequency band and *i-th* MIMO path, respectively. $f_{t,j}$ is the nonlinear function of input signals in different frequency bands, describes the output for j-th frequency band at i-th path. *i= 1,…,N*, *j = 1,…,B*, and *B* is the total number of frequency bands. The polynomial model for the complex output envelope in each band/path is expressed as:

$$y_{j\,[n]}^{(i)} = \sum_{t=1}^{N} \sum_{q=0}^{Q} \sum_{k_1=0}^{P} \dots \sum_{k_j=0}^{k_B} C_{j\,k_1,\dots,k_B,q}^{i,t}\, x_{j\,[n-q]}^{t}$$

$$\times \left|x_{1\,[n-q]}^{t}\right|^{k_1-k_2} \dots \left|x_{j\,[n-q]}^{t}\right|^{k_j-k_{j+1}} \dots \left|x_{B\,[n-q]}^{t}\right|^{k_B} \qquad (11)$$

In (11), each path is assumed to receive the crosstalk of all other paths in the MIMO structure. Typically, the coupling effects between those non-adjacent paths that are far from each other is negligible. Therefore, corresponding paths in *t=1,…,N* are neglected where there is a negligible coupling with the *i-th* path.

The total number of model coefficients for an N×N MIMO B-band transmitter is: $N \times B \times Q \times \binom{P/2}{B}$. In this expression, only the odd order of nonlinearity for even values of k_j is considered. Therefore, for a 2×2 dual-bad MIMO with *P=6* and *Q =4*, the total number of coefficients are: 160.

D. *System identification and DPD compensation*

Here, the MIMO multi-band system is presented in a matrix form, and the reverse form of the proposed model is considered as the DPD scheme.

By adopting linear algebra to develop a matrix form of (11), the forward model for an N×N MIMO multi-band transmitter in the presence of nonlinear crosstalk can be expressed as:

$$\left[\overrightarrow{y_J^{(1)}} \ \dots \ \overrightarrow{y_J^{(N)}}\right] = \left[\overrightarrow{Ax_J^{(1)}} \ \dots \ \overrightarrow{Ax_J^{(N)}}\right] \begin{bmatrix} \overrightarrow{h_J^{1,1}} & \dots & \overrightarrow{h_J^{1,i}} & \dots & \overrightarrow{h_J^{1,N}} \\ \vdots & & \overrightarrow{h_J^{i,t}} & & \vdots \\ \overrightarrow{h_J^{N,1}} & \dots & \overrightarrow{h_J^{N,i}} & \dots & \overrightarrow{h_J^{N,N}} \end{bmatrix} \qquad (12)$$

where $\overrightarrow{x_{J\,[n]}^{(i)}} = \left[x_j^i{}_{[1]} \quad \dots \quad x_j^i{}_{[L]}\right]^T$ and $\overrightarrow{y_{J\,[n]}^{(i)}} = \left[y_j^i{}_{[1]} \quad \dots \quad x_j^i{}_{[L]}\right]^T$ for L samples of the captured signal, $i = 1, \dots, N$, and also, the coefficient vectors are denoted by:

$$\overrightarrow{h_J^{i,t}} = \left[C_{j,10}^{i,t} \quad \dots \quad C_{j,Q}^{i,t}\right]^T \qquad (13)$$

$$C_{j,q}^{i,ii} = \left[C_j^{i,t}(0,\dots,0,q), \ \dots, \ C_j^{i,t}(k_1,\dots,k_B,q), \quad \dots, \quad C_j^{i,t}(P,\dots,P,q)\right]^T \qquad (14)$$

When we do not have crosstalk between the *i-th* and *t-th* paths, $\overrightarrow{h_J^{i,t}}$ =0.

Moreover, $\overrightarrow{Ax_j^i} = \left[\beta_{x_j^i}^{1} \cdots \beta_{x_j^i}^{q} \cdots \beta_{x_j^i}^{Q}\right]^T$ and $\beta_{x_j^i}^{q}$ are defined as matrices where their components are the input signals and all intermodulation distortion terms in the model. For example, for a dual-band system, $\beta_{x_j^i}^{q}$ is given as:

$$\beta_{x_j^i}^{q} = \left[x_j^i{}_{[n-q]} \cdots x_j^i{}_{[n-q]}\left|x_1^i{}_{[n-q]}\right|^{p-k}\left|x_2^i{}_{[n-q]}\right|^{k} \cdots x_j^i{}_{[n-q]}\left|x_2^i{}_{[n-q]}\right|^{P}\right]^T \qquad (15)$$

The model coefficients $\overrightarrow{h_J^{i,t}}$ can be estimated using the least square (LS) method and pseudo-inversing of the basis matrix in (12). In addition, by considering the DPD model as the inverse of forward model of the transmitter, the reverse model can be extracted simply by swapping the input and output signals [5].

Therefore, the coefficients of DPD, $\overrightarrow{d_j^{l,il}}$ as the complex DPD model coefficients, are calculated:

$$\vec{\mathrm{D}} = \mathrm{pinv}\left(\left[\overrightarrow{Ay_j^{(1)}} \ \ldots \ \overrightarrow{Ay_j^{(N)}}\right]\right)\left[\overrightarrow{x_j^{(1)}} \ \ldots \ \overrightarrow{x_j^{(N)}}\right] \quad (16)$$

where $\vec{D}$ is:

$$\vec{\mathrm{D}} = \begin{bmatrix} \overrightarrow{d_j^{1,1}} & \ldots & \overrightarrow{d_j^{1,i}} & \ldots & \overrightarrow{d_j^{1,N}} \\ \vdots & & \overrightarrow{d_j^{i,il}} & & \vdots \\ \overrightarrow{d_j^{N,1}} & \ldots & \overrightarrow{d_j^{N,i}} & \ldots & \overrightarrow{d_j^{N,N}} \end{bmatrix} \quad (17)$$

and $\mathrm{pinv}(\vec{F}) = (\vec{F}^{\,H}\,\vec{F})^{-1}\,\vec{F}^{\,H}$ denotes the pseudo-inverse of the matrix F.

3. Validation process and Measurement Setup

Owing to the limitation of available synchronous instruments in the lab, the proposed model is validated for two different scenarios: a 2×2 MIMO dual-band and a tri-band transmitter.

The block diagram of a 2×2 dual-band MIMO system with DPD in the presence of nonlinear crosstalk is shown in Fig 1.

In the measurement setup, all input signals must be synchronous [7], therefore, in the experimental setup, four and six synchronous vector signal generators (VSG) were required for the first and second scenarios, respectively.

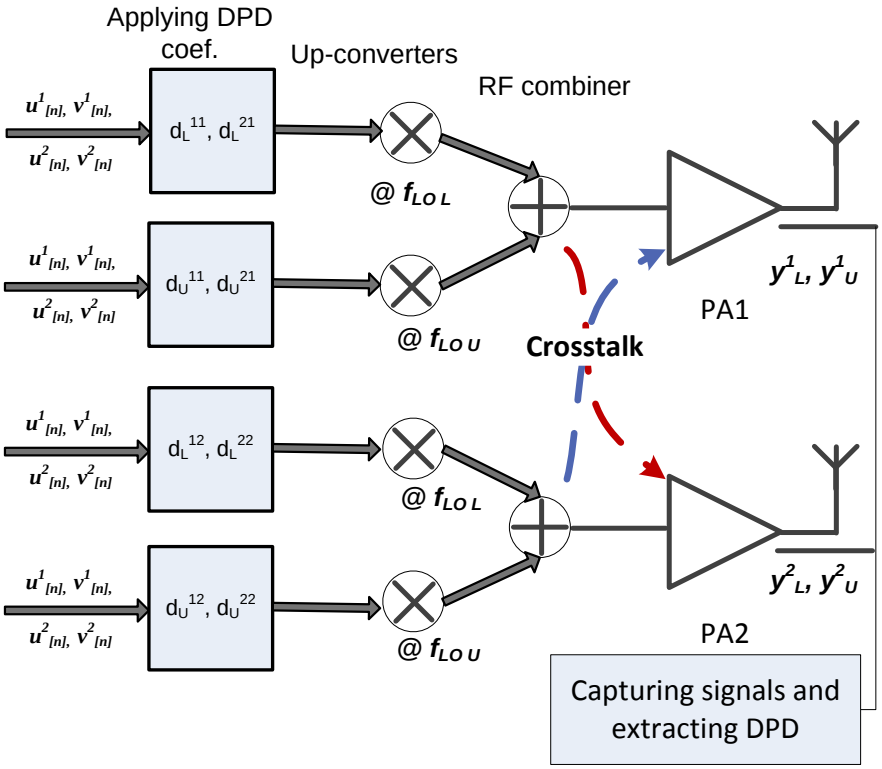

Fig. 1. The block diagram of a 2×2 dual-band MIMO system with DPD.

Due to the lack of enough number of synchronous VSGs in our lab, two VSGs were allocated to the MIMO paths. Hence, the complex envelope of input signals at lower, middle, and upper frequency bands for each MIMO path were shifted in frequency, aggregated in baseband, and then up-converted to RF. However, in this technique, the frequency separation between the bands is limited where the maximum sampling rate of VSG is 100 MHz. Since the performance of the proposed DPD architecture is completely independent of frequency separation between two carriers, it is apparent that this setup can be employed to validate the model.

In the first scenario (2×2 MIMO dual-band transmitter), four different 3 MHz LTE signals with 10.5 dB PAPR, sampled at 15.36 MHz, were considered as the input signals. Two synchronous VSGs (ESG 4438C) were utilized as DACs and frequency up-conversion units. For this purpose, the baseband signals assigned to the lower and upper bands were up-sampled to 92.16 MHz, shifted in frequency domain and aggregated in baseband. The carrier separation was chosen as 20 MHz. As a result, by up-converting the aggregated

signal to the RF using signal generators, the lower and upper bands of the dual band signals were set to 1940 MHz and 1960 MHz.

A similar process was deployed to generate the input signals for the second scenario, the MIMO tri-band transmitter. In this case, three different 3 MHz signals for each path were up-sampled to 92.16 MHz, shifted in frequency domain and aggregated in order to generate tri-band input signals with frequency spacing of 12 MHz. By loading the aggregated signals into the signal generators, the tri-band signals were generated at RF carriers of 1948 MHz, 1960 MHz, and 1972 MHz for the lower, middle and upper bands, respectively.

In order to artificially generate the crosstalk effect, the output signals of signal generators were connected with a coupler having -20 dB, and then were fed to the PAs. Fig. 2 shows the measurement setup used for validation of the proposed model.

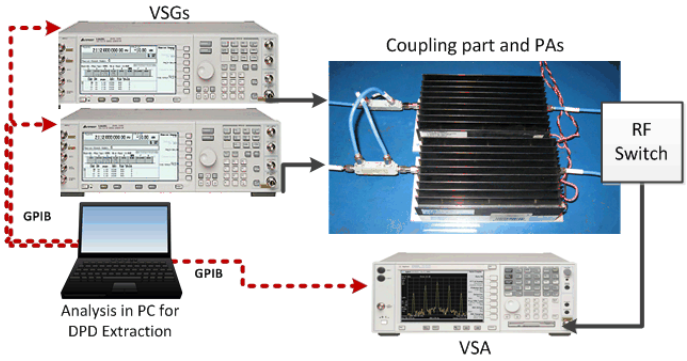

Fig. 2. Block diagram of the measurement setup.

Finally, the output signal of each frequency band for the first and second branches was captured separately using a vector signal analyzer (VSA 89650S). The VSA was used as a narrowband receiver to down-convert each band independently.

To compensate for the nonlinear distortion of MIMO dual/tri-band transmitters, 1) the distorted signals at the output of PAs for each branch/frequency band were captured separately, 2) the DPD model coefficients were extracted by a PC using LS method, 3) the DPD model was applied to the input signals separately and

then the distorted signal was aggregated and downloaded to the signal generators again, and 4) the output linearized signals of the transmitter after applying DPD were captured again.

4. Model Validation and Experimental Results

Two different scenarios, 2×2 MIMO dual-band and tri-band transmitters were considered in order to validate the proposed model. Normalized mean square error (NMSE) between the measured and estimated output signal of transmitter was calculated as a figure of merit to assess the accuracy of model. The NMSE of the reverse model indicates how well the proposed DPD model fits the physical system. For the first scenario (the MIMO dual-band transmitter), the performance of the DPD model for the dual-band case is demonstrated in Table I and Fig. 3.

TABLE I: NMSE of model and measured ACPR of output spectrum for dual-band MIMO system

Band/ MIMO branch	NMSE (dB)	ACPR (dBc) NO DPD	ACPR (dBc) With DPD
Lower Band /1st Branch	-45.2	-37.8	-57
Upper Band/1st Branch	-46.2	-37.5	-55.8
Lower Band/2nd Branch	-44.4	-37.2	-56.9
Upper Band/2nd Branch	-45.9	-36.4	-55.2

The accuracy of the inverse model for the lower and upper bands for each path in terms of NMSE is shown in Table I. Also, the normalized power spectral density (PSD) of the lower-band signal at the output of the second branch before and after experimentally applying DPD is illustrated in Fig. 3. The red and green spectra represent the results before and after applying the proposed DPD, respectively. Furthermore, the blue curve shows the spectra for the error between the input signal and the compensated output signal. It is evident that a more than 15 dB improvement in spectral regrowth suppression is achieved. The performance of the proposed DPD in other bands/branches was similar to Fig. 3. The adjacent channel power ratio (ACPR) as an appropriate metric to evaluate the nonlinear distortion was calculated and reported in Table I for all output signals.

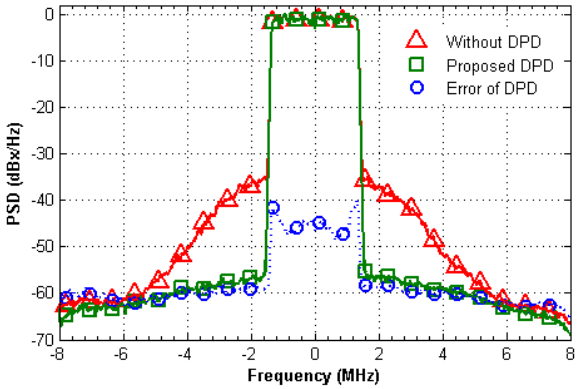

Fig. 3.Spectra of measured LB output signal of second path with -20 dB nonlinear crosstalk (red curve: without linearization; green curve: linearized with proposed DPD; and blue curve: error of DPD).

For the tri-band scenario, the accuracy of the model for the case of the MIMO tri-band transmitter is shown in Table II. Finally, the measured ACPR results for the captured signal before and after applying the proposed DPD are also provided in Table II. An ACPR better than -50 dBc was achieved using the proposed DPD.

TABLE II: NMSE of the model, and measured ACPR of the output spectrum for the tri-bad MIMO system

BAND/ MIMO BRANCH	NMSE (dB)	ACPR (dBc) NO DPD	ACPR (dBc) With DPD
Lower Band/1st Branch	-39.7	-38.3	-52.0
Middle Band/1st Branch	-38.8	-41.0	-51.4
Upper Band/1st Branch	-40.7	-39.0	-52.5
Lower Band/2nd Branch	-39.5	-38.0	-51.5
Middle Band/2nd Branch	-38.3	-41.2	-51.6
Upper Band/2nd Branch	-40.0	-40.8	-52.0

5. CONCLUSION

In this work, the nonlinear crosstalk in concurrent MIMO multi-band transmitters was investigated. The crosstalk was considered at the input of PAs. A novel DPD model for the linearization of the MIMO multi-band transmitter in the presence of nonlinear crosstalk was proposed. Moreover, an experimental 2×2

MIMO setup including two PAs in the presence of -20 dB crosstalk was utilized to validate the performance of the proposed model. For this purpose, two different scenarios for the dual-band and tri-band MIMO transmitter were implemented and compensated. The simulated and measured results confirmed that the model closely fits the system. By experimentally applying the proposed DPD, a significant spectral regrowth suppression, as well as an ACPR lower than -50 dB, was achieved.

REFERENCES

[1] M. Rawat, P. Roblin, C. Quindroit, K. Salam, C. Xie, "Concurrent Dual-band Modeling and Digital Predistortion in the Presence of Unfilterable Harmonic Signal Interference" in *IEEE Trans. Microw. Theory Techn*, vol. 63 no. 2, pp. 95-104, Feb. 2015.

[2] Amir Vaezi , A. Abdipour , A. Mohammadi “Analysis of nonlinear microwave Circuits excited by Multi-tone signals using Artificial Frequency Mapping Method”, Informacije MIDEM, Journal of Microelectronics, Electronic Components and Materials, Volume 41, Issue 3, September 2011, Pages 182-185,

[3] M. Rawat, P. Roblin, C. Quindroit, K. Salam, C. Xie, "Concurrent Dual-band Modeling and Digital Predistortion in the Presence of Unfilterable Harmonic Signal Interference" in IEEE Trans. Microw. Theory Techn, vol. 63 no. 2, pp. 95-104, Feb. 2015.

[4] X. A. Nghiem, J.Guan, T.Hone, and R.Negra, “Design of concurrent multiband doherty power amplifiers for wireless applications,” *IEEE Trans. Microw. Theory Techn.* , vol. 61, no. 12, pp. 4559–4568, Dec.2013.

[5] A. Bassam, M. Helaoui, and F. Ghannouchi, “Crossover digital predistorter for the compensation of crosstalk and nonlinearity in MIMO transmitters,” *IEEE Trans. Microw. Theory Techn.,* vol. 57, no. 5, pp.

[6] A. Bassam, M. Helaoui, and F. M. Ghannouchi, “2-D digital predistortion (2-D-DPD) architecture for concurrent dual-band transmitters,” *IEEE Trans. Microw. Theory Tech,* vol. 59, no. 10, pp. 2547–2553, October 2011.

[7] M. Younes and F. M. Ghannouchi, “On the modeling and linearization of a concurrent dual-band transmitter exhibiting nonlinear distortion and hardware impairments,” *IEEE Trans. Circuits Syst. I, Reg. Papers,* vol. 60, no. 11, pp. 3055–3068, Nov. 2013.

[8] S. Zhang, W. Chen, Y. Liu and F. M. Ghannouchi, "A Time Misalignment Tolerant 2D-Memory Polynomials Predistorter for Concurrent Dual-Band Power Amplifiers," IEEE Microwave and Wireless Components Letters, Vol. 23: Issue 9, pp. 501 - 503, September 2013.

[9] M. Younes and F. M. Ghannouchi, "Behavioral Modeling of Concurrent Dual-band Transmitters based on Radial-Pruned Volterra Model," *IEEE Communication Letters,* Vol. 19: Issue 5, pp. 751-754, May 2015.

[10] M. Younes, A. Kwan, M. Rawat and F. M. Ghannouchi, "Linearization of Concurrent Tri-Band Transmitters using 3-D Phase-Aligned Pruned Volterra Model *IEEE Trans. Microw. Theory Techn*., Vol. 61: Issue 12, pp. 4569-4578, December 2013.

[11] A. K. Kwan, M. Younes, F. M. Ghannouchi, S. Zhang, W. Chen, R. Darraji, M. Helaoui and O. Hammi, "Concurrent Multi-Band Envelope Modulated Power Amplifier Linearized Using Extended Phase-Aligned DPD," *IEEE Trans. Microw. Theory Techn*.,, Vol. 62: Issue 12, pp. 3298-3308, December 2014.

[12] M. V. Amiri, S. A. Bassam, M. Helaoui and F. M. Ghannouchi, "Estimation of Crossover DPD Using Orthogonal Polynomials in Fixed Point Arithmetic," *AEU International Journal of Electronics and Communications*, Vol. 67: Issue 11, pp. 905 - 909, November 2013.

[13]D. Saffar, N. Boulejfen, F. M. Ghannouchi, A. Gharsallah and M. Helaoui, "Behavioral Modeling of MIMO Nonlinear Systems with Multivariable Polynomials," *IEEE Trans. Microw. Theory Techn*., Vol. 59: Issue 11, pp. 2994-3003, November 2011.

[14] S. Amin, P. N. Landin, P. Handel, and D. Ronnow, "Behavioral modeling and linearization of crosstalk and memory effects in RF MIMO transmitters," *IEEE Trans. Microw. Theory Techn*., vol. 62, no. 4, pp. 810-823, April 2014.

[15] Y. Palaskas, A. Ravi, S. Pellerano, B. R. Carlton, M. A. Elmala, R. Bishop, G. Banerjee, R. B. Nicholls, S. K. Ling, N. Dinur, S. S. Taylor, and K. Soumyanath, "A 5-GHz 108-Mb/s 2×2 MIMO transceiver RFIC with fully integrated 20.5-dBm P_{1dB} power amplifiers in 90-nm CMOS," IEEE J. Solid-State Circuits, vol. 41, no. 12, pp. 2746–2756, Dec. 2006.

[16]Z. Fu, L. Anttila, M. Abdelaziz, M. Valkama and A. M. Wyglinski "Frequency-selective digital predistortion for unwanted emission reduction", *IEEE Trans. Commun.* , vol. 63 , no. 1 , pp.254 -267 , 2015